Neutron star-white dwarf mergers

early evolution, physical properties, and outcomes

Zenati, Y.; Perets, H.B.; Toonen, S.

DOI
10.1093/mnras/stz316

Publication date
2019

Document Version
Final published version

Published in
Monthly Notices of the Royal Astronomical Society

Citation for published version (APA):
Zenati, Y., Perets, H. B., & Toonen, S. (2019). Neutron star-white dwarf mergers: early evolution, physical properties, and outcomes. *Monthly Notices of the Royal Astronomical Society*, *486*(2), 1805-1813. https://doi.org/10.1093/mnras/stz316

Monthly Notices
of the
ROYAL ASTRONOMICAL SOCIETY

MNRAS **486,** 1805–1813 (2019)
Advance Access publication 2019 January 31

doi:10.1093/mnras/stz316

Neutron star–white dwarf mergers: early evolution, physical properties, and outcomes

Yossef Zenati,[1]★ Hagai B. Perets[1] and Silvia Toonen[1,2]

[1] *Physics Department, Technion – Israel Institute of Technology, Haifa 3200004, Israel*
[2] *Anton Pannekoek Institute for Astronomy, University of Amsterdam, Science Park 904, NL-1090 GE Amsterdam, the Netherlands*

Accepted 2019 January 28. Received 2019 January 18; in original form 2018 July 24

ABSTRACT

Neutron star (NS)–white dwarf (WD) mergers may give rise to observable explosive transients, but have been little explored. We use 2D coupled hydrodynamical-thermonuclear FLASH-code simulations to study the evolution of WD debris discs formed following WD disruptions by NSs. We use a 19-element nuclear network and a detailed equation of state to follow the evolution, complemented by a post-process analysis using a larger 125-isotope nuclear network. We consider a wide range of initial conditions and study the dependence of the results on the NS/WD masses (1.4–2 and 0.375–0.7 $\mathrm{M}_{\odot}$, respectively), WD composition (CO/He/hybrid He–CO), and the accretion-disc structure. We find that viscous inflow in the disc gives rise to continuous wind outflow of mostly C/O material mixed with nuclear-burning products arising from a weak detonation occurring in the inner region of the disc. We find that such transients are energetically weak (10^{48}–10^{49} erg) compared with thermonuclear supernovae (SNe), and are dominated by the (gravitational) accretion energy. Although thermonuclear detonations occur robustly in all of our simulations (besides the He WD), they produce only little energy (1–10 per cent of the kinetic energy) and ^{56}Ni ejecta (few $\times 10^{-4}$–10^{-3} $\mathrm{M}_{\odot}$), with overall low ejecta masses of $\sim$0.01–0.1 $\mathrm{M}_{\odot}$. Such explosions may produce rapidly evolving transients, much shorter and fainter than regular type Ia SNe. The composition and demographics of such SNe appear to be inconsistent with those of Ca-rich type Ib SNe. Though they might be related to the various classes of rapidly evolving SNe observed in recent years, they are likely to be fainter than the typical ones, and may therefore give rise to a different class of potentially observable transients.

Key words: stars: neutron – white dwarfs.

1 INTRODUCTION

The physical outcomes and observable expectations from mergers of neutron stars (NSs) and white dwarfs (WDs) are not well understood, and have been relatively little explored. Fryer et al. (1999) and King, Olsson & Davies (2007) suggested that accretion of the WD debris on a neutron star may produce a unique type of a long Gamma-ray burst (GRB). More recently, Metzger and collaborators (Metzger 2012; Fernández & Metzger 2013; Margalit & Metzger 2016a) studied the early accretion phase of the WD debris and the evolution of the accretion disc. They proposed that thermonuclear reactions can play an important role in the evolution of the disc, even prior to the final accretion of material on the NS, and suggested that such nuclear-dominated accretion can give rise to faint thermonuclear explosion occurring in the accretion disc (see also Margalit & Metzger 2016a, 2017). Here we follow these studies and explore NS–WD mergers and the evolution of the WD debris disc and the accretion-driven outflows through the use of more detailed and realistic models, which alleviate many of the potential difficulties and uncertainties in the previous models, as we describe below.

Fernández & Metzger (2013) employed 2D (axisymmetric) hydrodynamical simulations of radiatively inefficient accretion flows with nuclear burning. They studied the vertical dynamics of the disc and its interplay with the radially steady burning front. They found that the nuclear energy released at the burning front could be larger than the local thermal energy. When this condition is satisfied the burning front can spontaneously transition into an outwards propagating detonation, due to the mixing of hot downstream matter (ash) with cold upstream gas (fuel). Such detonations either falter once the shock propagates into the outer regions of the disc, or completely disrupt the large-scale accretion flow. However, Fernández & Metzger (2013) noted that the detonations they observe

---

★ E-mail: oyossefzm@gmail.com

Published by Oxford University Press on behalf of the Royal Astronomical Society

could be an artefact of their simplified equation of state (EOS), which included only gas pressure and neglected radiation pressure (thus artificially accentuating the temperature discontinuity at the burning front). Fernández & Metzger (2013) also employed only a single nuclear reaction, which prevented them from making detailed predictions for the composition of the disc outflows and their electromagnetic signatures. This also required them to add an ad hoc parameter so as to achieve more efficient nuclear burning required to ensue a detonation. Finally, they neglected the self-gravity of the disc, which could change the disc structure and evolution.

Similar to the approach introduced by Fernández & Metzger (2013), we follow the evolution of an accretion disc formed following the disruption of a WD by a NS, using simple, but physically motivated assumptions for the initial structure of the disc. We use the publicly available FLASH v4.2 code (Fryxell et al. 2000) to generate 2D hydro simulations of the disc, but we improve on the previous modelling in various aspects. In terms of the physical modelling, we include a detailed 19-element nuclear reaction network and a more realistic Helmholtz EOS, and we account for the self-gravity of the disc. These allow us to adequately and self-consistently capture the nucleosynthetic energetics without any ad hoc assumptions. In addition, we follow up the simulations with detailed post-process analysis of the nucleosynthetic products from the disc using an extended 125-isotope network.

Besides the more sophisticated models and the nucleosynthetic post-processing analysis, we also explore a wide range of initial conditions. We vary the NS and WD masses, as well as the WD composition (in particular considering hybrid – He–CO WDs), and we consider a range of initial accretion-disc configurations. Together these allow us to study the dependence of the outcomes of the disc evolution on a wide range of parameters. We generally find that the accretion-disc evolution robustly gives rise to weak thermonuclear explosions, but these produce little ^{56}Ni (at most 10^{-3} M$_{\odot}$), which, by themselves, could only give rise to very faint transients. Nevertheless, the accretion process releases much more significant energy; even a fraction of which could potentially give rise to a more energetic transient if converted to electromagnetic emission. The dependence of the outcomes on the initial configurations of such mergers is described in detail. Finally, 2D detailed simulations are too computationally expensive as to allow for long-term evolution studies as done in the simplified 1D disc simulations of Margalit & Metzger (2016a), however, we study a test case of a lower resolution long-term (30 s) simulation (Fig. 1).

We begin by describing our simulations and the various types of initial conditions we explored in Section 2, we then describe the main results in Section 3, and discuss and summarize them in Section 4.

2 METHODS AND INITIAL CONDITIONS

The evolution of a disrupted WD debris disc around a NS is simulated using the publicly available FLASH v4.2 code (Fryxell et al. 2000). The simulations were done using the unsplit PPM solver of FLASH in 2D axisymmetric cylindrical coordinates on a grid of size 1 × 1[10^{10} cm] using adaptive mesh refinement. We follow similar approaches as described in other works on thermonuclear SNe (e.g. Meakin et al. 2009). Detonations are handled by the reactive hydrodynamics solver in FLASH without the need for a front tracker, which is possible since unresolved Chapman–Jouguet detonations retain the correct jump conditions and propagation speeds. Numerical stability is maintained by preventing nuclear burning within the shock. This is necessary because shocks are artificially spread out over a few zones by the PPM hydrodynamics solver, which can lead to non-physical burning within shocks that can destabilize the burning front (Fryxell, Arnett & Müller 1989). In addition, we consider a wider range of initial conditions for the structure, mass, and composition of the disc, and we consider two different masses for the accreting NS.

We use a detailed EOS and account for the self-gravity of the disc. We also employ a 19-isotope reaction network, which burning front (Fryxell et al. 1989). In order to prevent the production of artificial unrealistic early detonation that may arise from insufficient numerical resolution, we applied a limiter approach following Kushnir et al. (2013).

We made multiple simulations with increased resolution until convergence was reached in the nuclear burning. We found a resolution of 1–10 km to be sufficient for convergence of up to 10 per cent in energy. Gravity was included as a multipole expansion of up to multipole $l = 12$ using the new FLASH multipole solver, to which we added a point-mass gravitational potential to account for gravity of the NS. We simulated the viscus term by using the viscosity unit in FLASH, employing a Shakura & Sunyaev (1973) parametrization $\nu_{\alpha} = \alpha C_{\rm s}^2/\Omega_{\rm Kepler}$, where $\Omega_{\rm Kepler}$ is the Keplerian frequency and $C_{\rm s}$ is the sound speed, and the α parameter used is 0.01. The contributions of both nuclear reaction and neutrino cooling (Chevalier 1989; Houck & Chevalier 1991) are included in the internal energy calculations, and the Navier–Stokes equations are solved with source terms due to gravity, shear viscosity, and the nuclear reactions.

The EOS used in our simulations is the detailed Helmoholz EOS employed in FLASH (Timmes & Swesty 2000). This EOS includes contributions from partially degenerate electrons and positrons, radiation, and non-degenerate ions. It uses a look-up table scheme for high performance. The most important aspect of the Helmholtz EOS is its ability to handle thermodynamic states where radiation dominates, and under conditions of very high pressure.

The nuclear network used is the FLASH α-chain network of 19 isotopes. This network can adequately capture the energy generated during the nuclear burning (Timmes & Swesty 2000). In order to follow the post-process analysis of the detailed nucleosynthetic processes and yields, we made use of 4000–10 000 tracer particles that track the radius, velocity, density, and temperature and are evenly spaced every 2×10^8 cm throughout the WD debris disc. Our simulations are evolved for 7–13 s. In one test case, we run a lower resolution evolution up to 30 s. Following the FLASH runs, we make use of the detailed histories of the tracer particles density and temperature to be post-processed with MESA (version 8118) one-zone burner (Paxton et al. 2015). We employ a 125-isotope network that includes neutrons (see supplementary information), and composite reactions from JINA's REACLIB (Cyburt et al. 2010). Overall we find that the results from the larger network employed in the post-process analysis show less efficient nuclear burning (it is negligible), giving rise to somewhat higher yields of intermediate elements on the expense of lower yields of iron elements, similar to the results seen in other works (García-Senz et al. 2013; Papish & Perets 2016).

2.1 Initial disc properties

We focus on discs that form when a WD is tidally disrupted by a companion NS in a close binary system (Fryer et al. 1999). We first review the characteristic properties of the discs, closely following Fernández & Metzger (2013). Whether the WD is disrupted by the NS depends on stability of the mass-transfer process following

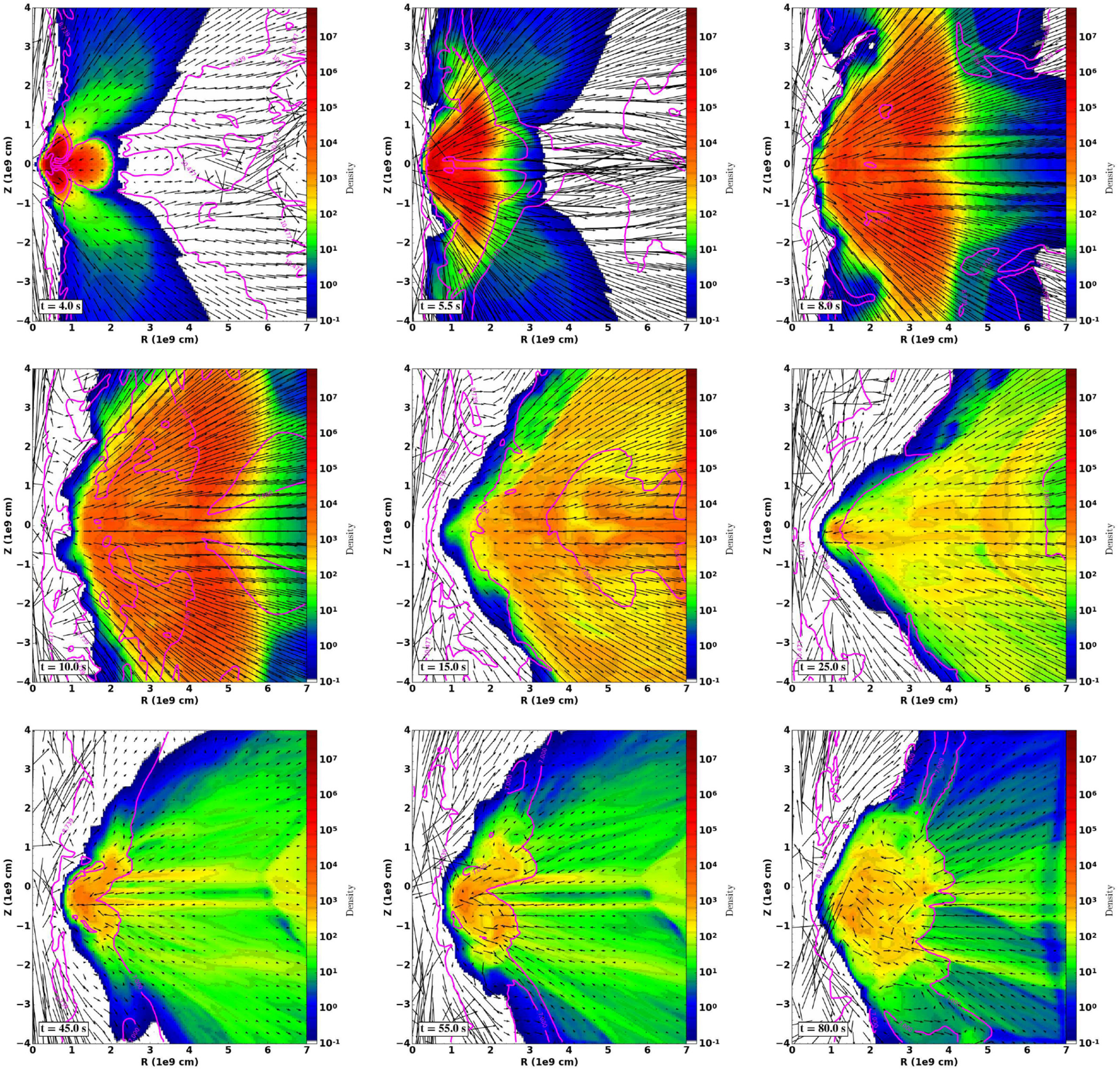

Figure 1. The long-term evolution of the WD debris outflows (similar to Fig. 2) in from the low-resolution simulation of model E. There are three different velocity scales 5000, 4600, and 3000 km s^{-1} for three different epochs 0–5, 5–20, and 25–80 s, respectively.

the onset of Roche lobe overflow. Once the WD is disrupted, the conservation of angular momentum implies that the material will circularize around the NS at a characteristic radius

$$R_0 = \frac{a_{\rm RLOF}}{1+q}, \tag{1}$$

where $a_{\rm RLOF} = f \cdot R_{\rm WD}$, $0.4 < f < 0.8$, $R_{\rm WD}$ is the radius of the WD, and the mass ratio of the binary is given by $q = M_{\rm WD}/M_{\rm NS}$. The orbital time at the circularization radius is

$$t_{\rm orb} \simeq 38 \left(\frac{R_0}{10^{9.3}\,{\rm cm}}\right)^{3/2} \left(\frac{M_{\rm NS}}{1.4\,{\rm M}_{\odot}}\right)^{-1/2} {\rm s}\,. \tag{2}$$

The characteristic time-scale for matter to accrete is estimated by the viscous time and the characteristic accretion $\dot{M} \sim M_{\rm WD}/t_{\rm visc}$. Following Stone, Pringle & Begelman (1999) and Fernández & Metzger (2013), the torus density is normalized to its maximum value $\rho_{\rm max}$, thereby fixing the polytropic constant in terms of the adiabatic index and the torus distortion parameter d. The latter is a measure of the internal energy content of the torus and the scale height H_0 (Stone et al. 1999; Fernández & Metzger 2013). We then get

$$\rho_{\rm disc} = \rho_{\rm max} \left[\left(\frac{2H}{R_0}\right) \frac{2d}{d-1} \left(\frac{R_0}{r} - \frac{1}{2}\left(\frac{R_0}{r\sin\theta}\right)^2 - \frac{1}{2d} \right) \right]^{7/2} \tag{3}$$

$$\frac{P}{\rho} = \frac{2GM}{5R_0} \left[\frac{R_0}{r} - \frac{1}{2}\left(\frac{R_0}{r\sin\theta}\right)^2 - \frac{1}{2d} \right]. \tag{4}$$

Note we would improve on Fernández & Metzger (2013), who have not accounted for the self-gravity of the disc. Fernández & Metzger (2013) used a simplified $\gamma = 5/3$ EOS and did not solve for the value of d, and considered three somewhat arbitrary specific values. In contrast, we have self-consistently derived the structure of the disc, by first choosing initial values for the parameters in equation (3) like Fernández & Metzger (2013), but then we derived the actual EOS given the disc conditions in FLASH. We then rederived the structure of the disc using the new EOS parameters. We iterated this procedure until the structure converged, i.e. the EOS and the density distribution in each of the disc region cells in FLASH did not change (to the level of 10^{-5}) between consecutive iterations. We find that our more consistent model for disc structure, accounting for more realistic EOS, and the self-gravity produce more compact discs than assumed by Fernández & Metzger (2013).

We assume that the internal energy is dominated by non-degenerate particles, and that it balances 25 per cent of the gravitational energy; this assumption derives from the virial theorem. Note that the opacity is dominated by electron scattering and the diffusion time-scale for photons that escape the disc is much longer than the time-scale for the disc formation $t_{\rm diff} \gg t_{\rm orb}$, and $t_{\rm visc}$, where $t_{\rm visc}$ is the viscous time-scale

$$\begin{aligned} t_{\rm visc} &\simeq \alpha^{-1}\left(\frac{R_0^3}{GM_{\rm c}}\right)^{1/2}\left(\frac{H_0}{R_0}\right)^{-2} \\ &\sim 2600\,{\rm s}\left(\frac{0.01}{\alpha}\right)\left(\frac{R_0}{10^{9.3}\,{\rm cm}}\right)^{3/2}\left(\frac{1.4\,{\rm M}_{\odot}}{M_{\rm c}}\right)^{1/2}\left(\frac{H_0}{0.5R_0}\right)^{-2}, \end{aligned} \tag{5}$$

where α parametrizes the disc viscosity.

Neutrino cooling (included in our simulations) does not play an important role. Even at the hottest and most dense regions, we find that the time-scale for neutrino cooling is far longer than the simulation time. We further validated this through running similar simulations without neutrino cooling – the results show essentially no difference from the simulation that did include this process.

2.2 WD debris disc and NS models

The detailed properties of each of the NS–WD models we explored are described in Table 1. The mass and composition of the WD debris models we consider are determined by the properties of the WD progenitors of the disc. The properties of the WDs are obtained through detailed stellar evolution models of single and binary stars using the MESA code (Paxton et al. 2011, 2015). In all cases, we considered only Solar metallicity stellar progenitors. Our models include both typical CO WDs as well as hybrid HeCO WDs. The former are produced from the regular evolution of single stars, which eventually produce WDs composed of ∼50 per cent carbon and ∼50 per cent oxygen. The hybrid WDs, containing both CO and He, are derived from detailed *binary* evolution in MESA, as described in Zenati, Toonen & Perets (2018). We also considered several artificial WD compositions with higher He fractions than produced in our models. Though these may potentially arise from accretion of He on a WD under some complex binary evolutionary scenarios, we stress that these have significantly less physical motivation from stellar evolution models, and should be considered with a grain of salt.

The NSs are not resolved in our simulations and only participate in the simulations as point masses/potentials. We considered two NS masses, 1.4 and 2 $\rm M_{\odot}$. Together the NS mass and the WD structure (mass and composition) determine the tidal radius at which a given WD is expected to be disrupted [$r_{\rm t} \sim (M_{\rm NS}/M_{\rm WD})^{1/3}R_{\rm WD}$, where $M_{\rm NS}$, $M_{\rm WD}$, and $R_{\rm WD}$ are the NS mass, WD mass, and WD radius, respectively]. The disc outer radius is assumed to be positioned near the tidal radius, but we have explored a range of specific inner disc radii (see the table).

Simulations of WD disruptions by stellar compact objects (e.g. Fryer & Woosley 1998; Dan et al. 2012) suggest that very thick discs are produced, but the exact structure of the disc is not known. We therefore considered two disc heights $H/R_0 = 0.5$ and 0.7. The initial structure of the disc is assumed to follow a Shakura–Sunyaev structure, as described above. Note that we find that the self-gravity of the disc, not included in previous studies, can significantly alter the structure of the disc even before significant radial evolution occurs in the disc. The effects of the self-gravity become more pronounced for smaller disc heights.

3 RESULTS

Our main results are summarized in Table 2 where the overall properties of the simulated models are described. The cases of He WDs did not give rise to any thermonuclear explosive event, nor to outflows; the disc expanded but no mass was ejected from the system, nor any nuclear burning occurred on the time-scales of our simulations. We therefore do not further discuss these models that appear to produce a peculiar but non-explosive object; the long-term evolution of such objects is worth exploring, but is beyond the scope of this paper. In the following, we discuss the evolution of the other models and their outcomes in more detail.

Though the disc evolution and final outcomes depend on the specific model or initial conditions, the overall evolution of the discs we modelled follows a very similar evolution, and we focus on one example shown in Fig. 2. As can be seen in the snapshots, the disc evolves radially through viscous evolution; the inner regions of the disc spread inwards, while the outer regions expand outwards. At the same time, the inner parts of the disc gravitationally collapse vertically to form a thinner structure. As the inner disc evolves into a more compact and thinner configuration its density and temperature increase. Material then accretes inwards through the (horizontal) central parts of the disc and outflows of material ensue after a few seconds. The outflows are ejected at a wide angle from the innermost central parts, as gravitational accretion energy is converted into heat and kinetic energy fuelling the outflows. The fastest and hottest material is funnelled almost vertically from the innermost parts of the accretion disc, producing a jet-like structure with velocities extending up to $\sim 3 \times 10^4\,{\rm km\,s^{-1}}$, but enclosing only a small fraction of the ejected material.

Note that material is accreting inwards throughout the simulation, but the main accretion happens at early times, until heated material in the inner regions gives rise to significant pressure and outflows. These in turn choke further significant accretion, which then happens only stochastically and only through low-rate infall of material. At these later times outflows from the inner region counteract most of the inflow in the disc, producing a region where material is stalled at about 2.5×10^8 cm. Note that the inner regions show apparently 'empty' regions, but as shown by the velocity arrows are not empty but rather correspond to lower densities below the colour coding resolution.

As the density and temperature increase in the inner regions, they attain the critical conditions for thermonuclear burning, and an explosive weak detonation occurs. However, only a small fraction of the accreting material participates in the thermonuclear burning and therefore little amounts of nucleosynthetic by-products are produced, with only up to $\sim 10^{-3}$–$10^{-2}\,{\rm M}_{\odot}$ of material is burnt into intermediate or even iron elements. In particular, at most $10^{-3}\,{\rm M}_{\odot}$ of

Table 1. The parameters of the simulated NS–WD merger models. $M_{\rm WD}$ is the mass of the disrupted WD. $M_{\rm NS}$ is the mass of the NS. $\rho_{\rm max}$[g] is the maximum density in the debris disc. $R_0/r_{\rm t}$ is the distance of the innermost edge of the disc in units of the tidal-disruption radius. ν cooling describes whether neutrino cooling was considered. H/R_0 is the height scale of the disc. %He$_4$, %C$_{12}$, and %O$_{16}$ are the fractions of He, C, and O composing the disc, respectively.

#	$M_{\rm WD}$	$M_{\rm NS}$	$\rho_{\rm max}$[g]	$R_0/r_{\rm t}$	ν cooling	H/R_0	%He$_4$	%C$_{12}$	%O$_{16}$
A*	0.53	1.4	1.9×10^6	1.1	Yes	0.5	–	50	50
B	0.5	1.4	5.5×10^6	0.8	No	0.5	–	50	50
C	0.55	1.4	8.5×10^6	0.8	No	0.5	–	50	50
D	0.62	1.4	6.4×10^6	1	No	0.5	9	50	41
E†	0.62	1.4	8.5×10^6	0.8	No	0.5	4	49	47
F	0.62	2.01	2.3×10^6	1.1	Yes	0.5	–	50	50
G	0.73	1.4	2.1×10^7	1	No	0.5	–	50	50
H	0.73	2.01	4.9×10^5	2	No	0.5	–	50	50
I	0.73	1.4	1.1×10^7	1	No	0.7	–	50	50
J*	0.8	1.4	4.4×10^7	0.8	No	0.5	–	50	50
K	0.28	1.4	5.2×10^4	1.1	No	0.5	100 per cent	–	–
L	0.28	1.4	1.3×10^4	2	No	0.5	100 per cent	–	–

Notes. *These models were run both with and without neutrino cooling, with no differences observed. †These models were also run for longer time, but at a lower resolution.

Table 2. The final outcome simulations and contains a collection of their properties, the composition of the material and their energy that remains gravitationally bound and eventually will mix with the remnant WD. The C/O, IME, IGE and the Ni amount for Bound (B) and Unbound material (U) and the thermal and nuclear and kinetic energy.

#	$M_{\rm WD}$ (M$_\odot$)	$E_{\rm thermal}$ (erg)	$E_{\rm nuc}$ (erg)	^{56}Ni$_{\rm B}$ (M$_\odot$)	$E_{\rm K}$ (erg)	(C/O)$_{\rm B}$ (M$_\odot$)	IME$_{\rm B}$ (10^{-3} M$_\odot$)	IGE$_{\rm B}$ (10^{-3} M$_\odot$)	(C/O)$_{\rm U}$ (10^{-3} M$_\odot$)	IME$_{\rm U}$ (10^{-3} M$_\odot$)	IGE$_{\rm U}$ (10^{-3} M$_\odot$)	$M_{\rm Tot\text{-}U}$ (10^{-3} M$_\odot$)
A	0.53	4.8×10^{46}	3.2×10^{47}	3.1×10^{-3}	3.5×10^{48}	0.49	11	5.7	11	9.0	4.0	24
B	0.5	1.5×10^{46}	9.7×10^{46}	4.52×10^{-3}	6.1×10^{48}	0.42	36	0.3	34	3.8	6.1	45
C	0.55	8.2×10^{45}	2.6×10^{46}	5.25×10^{-3}	2.8×10^{48}	0.49	40	0.44	9.5	0.5	9.0	19
D	0.62	9.4×10^{45}	8.1×10^{47}	6.16×10^{-3}	3.6×10^{49}	0.46	28	8.5	120	85	9.6	210
E	0.62	2.3×10^{46}	6.9×10^{47}	2.84×10^{-3}	1.4×10^{49}	0.48	57	24	30	23	6.1	90
F	0.62	7.7×10^{45}	2.4×10^{46}	3.38×10^{-3}	1.5×10^{48}	0.52	76	17	4.8	0.1	3.3	8.1
G	0.73	1.8×10^{46}	8.8×10^{46}	2.68×10^{-3}	1.2×10^{49}	0.65	19	9.1	25	23	3.8	52
H	0.73	1.1×10^{45}	2.8×10^{45}	2.91×10^{-3}	9.1×10^{47}	0.69	32	1.8	2.8	0.3	0.5	3.6
I	0.73	7.5×10^{45}	2.1×10^{46}	8.25×10^{-4}	2.5×10^{48}	0.64	66	8.9	2.9	5.5	1	9.4
J	0.8	6.2×10^{46}	5.9×10^{47}	1.78×10^{-3}	3.2×10^{49}	0.60	82	24	40	7.0	45	94

^{56}Ni is produced, and only little nuclear energy ($\sim$few $\times 10^{46}$–10^{47} erg) is produced during the process (see Table 2). For a comparison, 10–100 times larger gravitational energy ($\sim$ few $\times 10^{47}$–10^{49} erg) is released, driving the outflows and heating of the material. In other words, nuclear processes appear to play a relatively minor role in the overall evolution of the debris-disc evolution and outflows. In particular, a model run without and nuclear interactions gave rise to very similar kinematic results compared with its counterpart run that included nuclear burning, with the main difference being a small fraction of ejected burnt material in the latter run.

The computational expense limits the length of our simulations. However, as a test case we run two of our simulations at lower resolution and followed them on a larger simulation box, better allowing us to follow the long-term evolution of the outflows. As can be seen in Fig. 2, the early evolution followed by both the low- and high-resolution simulations is qualitatively similar, suggesting that the low-resolution models reasonably follow the NS–WD evolution. The long-term evolution shows that after the first 10 s or so outflows transform the initially thin disc into a puffy structure around the NS with extended outflows ejecting a few per cent of the WD debris. The long-term evolution of the now more spherical cloudy structure of the leftover debris around the NS is beyond the scope of our models, to be studied elsewhere (Fig. 1).

We note that the comparison between the low-resolution long-term models with the high-resolution short-term simulations suggests that the overall energetics and mass-loss in the short-term models represent only about half of the total energetics/outflows arising from the merger.

In Fig. 3, we show the mass-loss evolution for the various models. It shows the results from the high-resolution simulations run up to 8–12 s. For model E, we also run a longer term, but lower resolution simulation up to 80 s, which compares well with its low-resolution counterpart simulation. As can be seen, the outflow rate increases to peak after a few seconds and then decreases back to a negligible level.

We analyse the rate of mass crossing the closest region near the NS resolved in our simulations (2×10^8 cm), in order to provide an upper limit on the accretion rate on to the NS. We cannot resolve the size of the NS, however, even assuming that all the mass that crosses into this region accretes on the NS, the total mass accreted is small, not more than 10^{-4} M$_\odot$, not likely to produce a typical or even a subluminous GRB.

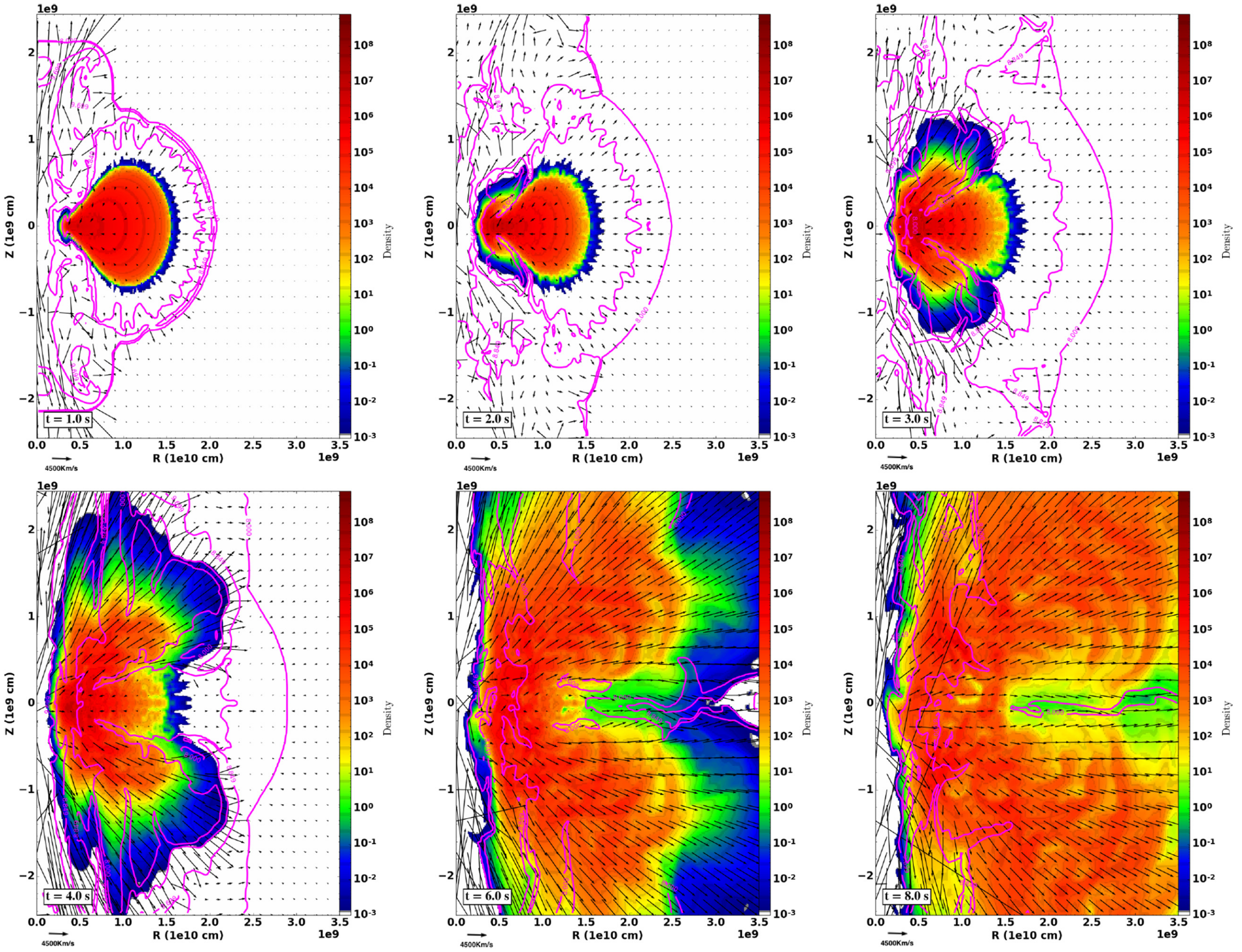

Figure 2. The evolution of the WD debris at early times for model E, modelled at high resolution. Each panel shows the (colour coded) density distribution and velocity vectors (black arrows) at different times. The velocity scale is 4500 km s^{-1}. The magenta contours correspond to the temperature.

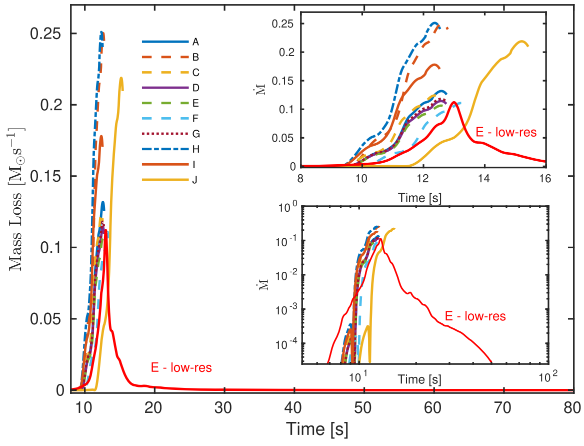

Figure 3. The rate of mass-loss from the system (unbound material) in each of the models as a function of time. The subplots show a zoom-in of the same evolution at early times, and the same on logarithmic scale. Both short-term high-resolution and long-term low-resolution simulations are shown for model E.

4 DISCUSSION

4.1 Energetics and composition

As described above, the energetics and outflows in the NS–WD merger we modelled are dominated by accretion energy and not by the nuclear processes involved. Therefore, the most energetic cases that are also expected to produce the largest ejected masses are those in which the most gravitational energy is released. This leads to several trends: generally, the more massive the WD debris and the NS are, the more energetic are the outflows and the thermonuclear energetics. Note, however, that the inner radius of the debris disc also plays an important role. Immediately following the WD disruption the system is not in a steady accretion state, and the inner regions are initially empty. The position of the inner initial region of the debris disc is chosen as to coincide with the appropriate tidal radius given the NS and WD properties. However, the exact structure of the debris disc is more complex than our simplified models and we therefore checked the dependence of slightly by moving the disc position inwards or outwards (see $R_0/r_{\rm t}$ in Table 2). As we show, the results depend on the chosen inner positions, but the overall behaviour is robust and is not strongly dependent on the exact choice. Closer-in debris discs are more effective in allowing for material to accrete into close-in orbits before outflows become efficient enough to quench further accretion. The overall ejected mass and total energetic are therefore determined by both the overall NS and WD mass and the inner radius of the disc; these are well reflected in Table 2.

Overall the *nuclear* energy deposited increases with increasing density and with Helium content. These provide more favourable conditions for nuclear burning. The density is determined by the total mass of the debris disc (the disrupted WD), the inner radius (r_d), the disc scale height, and to some extent the disc composition that affects the EOS (see equation 3). As can be seen in Table 2, the nuclear energy produced follows these various trends; it increases with increasing WD mass and Helium content, as well as with decreasing disc scale height and inner radius. The tidal radius, which determines the inner radius, depends on both the NS mass and the WD mass, as well as on the WD composition, and hence more massive NSs (giving rise to larger tidal radii) correspond to lesser production of nuclear energy. The pure Helium WD case (not shown) is the only case where no nuclear burning is observed. This may appear counter-intuitive given the lower temperatures and densities required to ignite Helium, however such WDs have a lower mass and are much puffier, hence the effective density of the debris disc they produce is far lower than that of CO WD debris disc, explaining the result.

As discussed above, our results suggest that only a small fraction of the WD debris disc is effectively ejected during the modelled evolution, while most of the material expands to produce a more isotropic configuration, but stays bound to the NS. The long-term evolution of such expanded debris ‘atmosphere’ is beyond the scope (and computational capabilities) of the current study focusing on the immediate outcomes of the merger following the disruption of the WD.

As already noted, nuclear burning is not the main driver of the outflows in NS–WD mergers, and only a small fraction of the WD debris disc experiences any nuclear burning. Hence, the majority of the ejected unbound material (identified through the comparison of the kinetic and potential energy of each mass element) shows the same composition as the original WD, i.e. C/O composition (and He in the hybrid WD cases). However, most of the unbound material is ejected through outflows from the inner regions, where most of the nuclear burning occurs, and therefore, although most of the ejected material is composed of C/O, it still contains a significant, sometimes comparable, fraction of burned material. The latter is typically composed of both intermediate and Iron group elements at comparable levels (Table 2; see the composition table in the supplementary information for the more detailed composition). A comparison of the results from the 19-isotope network and the extended 125-isotope network shows very small, negligible differences when comparing the abundances of the same isotopes.

4.2 Observational properties

4.2.1 Gamma-ray burst

The total mass accreted on the NS in our simulations appears to be small, as was also found by Metzger and collaborators (Fernández & Metzger 2013; Margalit & Metzger 2016b), suggesting that such mergers are not likely to produce regular GRBs, though one cannot exclude ultrafaint long GRBs extending for time-scale comparable to the accretion time-scale of typically a few seconds.

4.2.2 Optical transients

Our overall results give rise to comparable ranges of ejected masses, velocities, and production of ^{56}Ni as found in the simplified 1D model of Margalit & Metzger (2016a). Consequently, the observable expectations are the same, namely the production of fast-evolving, very faint transients, which should peak at typical time-scales of 6–7 d, and peak bolometric luminosity of 10^{40}–10^{41} erg s^{-1}. Note, however, that our multidimensional findings allow us to consider the overall structure of the ejecta. We find that the structure of the outflows has a highly non-spherical configuration, with most of the material ejected at intermediate inclinations, and little mass ejected from the poles in a jet-like configuration with a few times higher velocity than the typical ejecta. The latter ‘jet’-ejecta contains a higher ^{56}Ni fraction per unit mass compared with the rest of the ejecta. The observational features of such NS–WD mergers could therefore significantly vary as a function of the viewing angle.

Given their expected rapid evolution, such transients could be related to the class(es) of fast-evolving SNe (de Vaucouleurs & Corwin 1985; Kasliwal et al. 2010; Poznanski et al. 2010; Perets et al. 2011; Drout et al. 2013, 2014), however, they are likely to be too faint to explain the majority of the luminous fast-evolving SNe observed; if at all they are more likely to be related to the faint end of such SNe such as SN 2010X. Nevertheless, they might be too faint to even explain 2010X-like SNe, and both their Helium and Aluminium content is small and may not explain the He and Al lines identified in that SN (Kasliwal et al. 2010). Transients from NS–WD mergers may therefore present a completely different class of SNe, which might be observed mostly in close-by galaxies using large telescopes, possibly with next-generation surveys such as LSST.

As we show in Toonen et al. (2018), the rates of NS–WD mergers could be comparable to the inferred rate of fast-evolving SNe (Drout et al. 2014), and the delay-time distributions show them to peak at early times of hundreds of Myr up to a Gyr, suggesting their typical host galaxies to be late-type disc galaxies. We find that only a small fraction of the mergers involve hybrid WDs (Zenati et al. 2018) that may give rise to some He ejection as observed in 2005E-like Ca-rich gap transients (Perets et al. 2010). These low rates and delay-time distributions peaking at early times, together with the extremely low luminosity and very little Ca production we find, likely exclude NS–WD mergers as progenitors of the type Ib 2005E-like Ca-rich gap transients (Perets et al. 2010). The latter show clear evidence for He, are Ca-rich, explode at high rates (Perets et al. 2010; Frohmaier et al. 2018) and mostly explode at early-type galaxies and old environments (Perets et al. 2010; Kasliwal et al. 2012; Lyman et al. 2013) inconsistent with our findings for NS–WD mergers.

4.2.3 Comparison with previous work

The detailed studies most comparable with our work are those by Fernández & Metzger (2013) and Margalit & Metzger (2016a). The former used a short-term 2D FLASH simulation similar to ours, but used a simplified EOS and a single nuclear reaction. They also did not consider the self-gravity of the disc, and did not make a detailed post-analysis of the detailed composition. These issues required them to use ad hoc assumptions regarding detonations that could not be resolved from the simulations. They also could not provide a detailed composition analysis as done here. The latter work by Margalit & Metzger (2016a) explores a simplified 1D model for the WD debris disc. Such a model required them to use various assumptions regarding the wind ejection, which cannot be resolved in such models, and could not explore multidimensional structure of the ejecta, however, it allowed them to provide detailed models for the composition structure of the disc, and follow its evolution up to late times.

Our models are therefore complementary to both these previous works and extend them in several aspects. Our detailed 19-element nuclear network resolves the issues of nuclear energy and robustly shows that weak nuclear detonations are indeed produced, supporting the previous models, albeit with somewhat lower energetics than envisioned by Fernández & Metzger (2013). We also find that the self-gravity of the disc, not included before, can significantly affect its evolution (see Fig. 4), and the overall effects of the detailed nuclear network, detailed EOS, and self-gravity give rise to somewhat smaller energy contribution from the thermonuclear burning than suggested by the early study of Fernández & Metzger (2013). Our long-term, lower resolution models bridge the gap between the short-term 2D models at early times explored by Fernández & Metzger (2013) and the 1D long-term models by Margalit & Metzger (2016a), by allowing detailed 2D simulations extending to late times (Fig. 1). These results and our post-analysis detailed 125-element composition studies allow for a comparison with the Margalit & Metzger (2016a) study. Overall we find a good qualitative and quantitative consistency between the overall composition results. Our models could therefore also be used as self-consistent models to calibrate the hitherto assumed properties of winds in 1D models. Moreover, our models also include details on the structure of the wind and its jet-like polar configuration.

Note that the direct comparison with Margalit & Metzger (2016a) is more difficult, given the different dimensionality and the very different assumptions taken. It is therefore difficult to say whether we should have expected exactly the same behaviour. In particular, we see significantly less accretion into the inner regions than found by them, though we should note that the typical grid boundary in our simulations is in the range of (1–2) × 10^8, i.e. we do not resolve the innermost regions at the level possible in 1D models. Our simulations, however, do show significant nuclear burning and outflows at much larger scales than found in Margalit & Metzger. This might not be surprising, since our simulations self-consistently resolve both the radial and vertical structures, unlike the 1D models, and the evolution could differ. In particular, following the inner collapse of the disc (neither modelled in the 1D simulations, nor captured by the simulation of Fernandez & Metzger (2013), which did not include the self-gravity of the disc), the densities and temperatures become very high already at much larger scales than our resolves 10^8 cm, and are sufficiently high for the initiation of nuclear burning.

In summary, our models explored various regimes and initial conditions not explored before, enabling us to study the dependence of the merger outcomes on the WD composition and mass, as well as on the detailed structure of the WD debris disc. Though our models cannot resolve the innermost regions close to the NS, as can be done in 1D simulations, they more self-consistently resolve the disc evolution and the wind mass-loss without introducing assumptions on the vertical evolution of the disc, nor on the wind mass-loss as in the 1D simulation. Our result suggests that nuclear burning initiates already at larger scales, and that the accretion to the inner regions is significantly smaller than inferred from the 1D simulations.

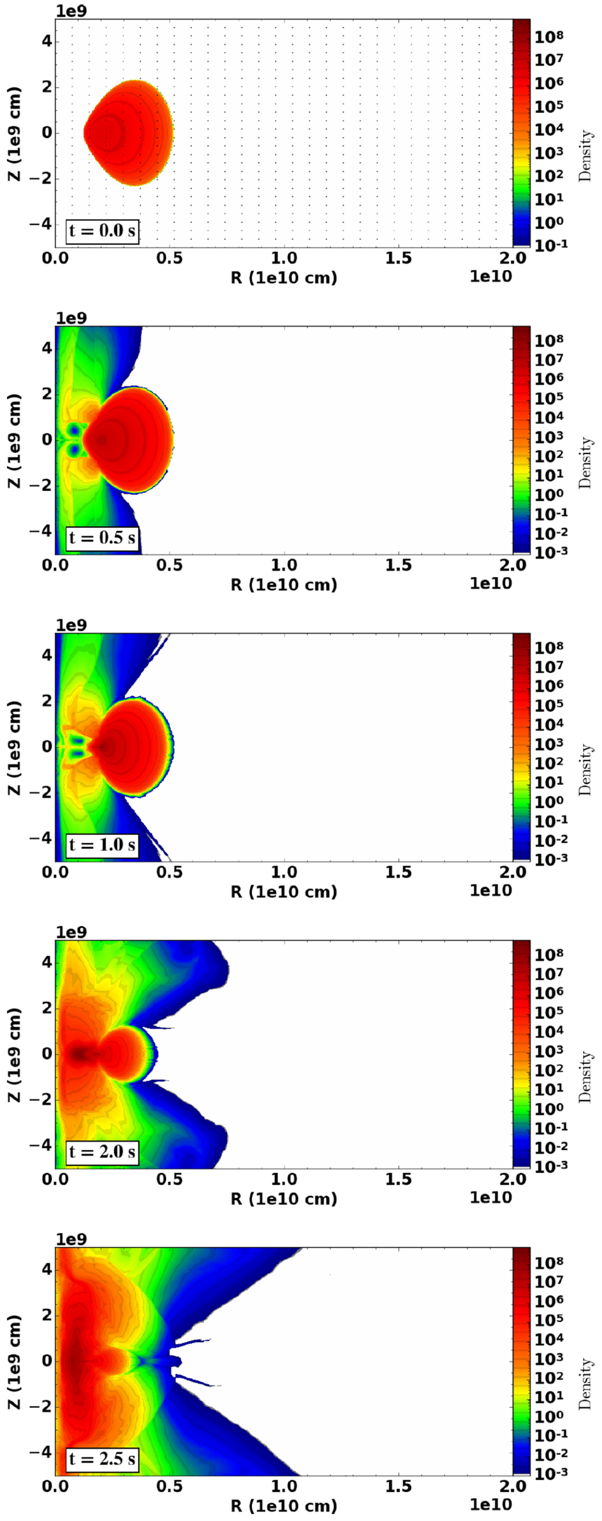

Figure 4. The evolution of the WD debris at early times for a similar model as studied and shown in fig. 1 of Fernández & Metzger (2013), but including self-gravity. As the disc evolves, its inner parts collapse, producing a 'pinched'-like structure, not seen in the simulations without the self-gravity of the disc. A similar type of evolution is seen in all of our simulations.

5 SUMMARY

In this study, we explored the early-time evolution of NS–WD mergers using a 2D hydrodynamical simulation of the debris disc of a disrupted WD around a NS. We made use of an extended nuclear network to follow nuclear burning in such models, and explored a wide range of initial conditions and combinations of masses and compositions of NSs and WDs. We find that such mergers are mostly driven by the gravitational energy released in the accretion process, giving rise to mass ejection through strong winds launched from the inner regions of the accretion disc. These produce a 'jet'-like configuration of fast polar winds, which eject little mass, and somewhat slower winds at intermediate inclinations, which carry most of the ejected material. We find support for earlier claims that weak nuclear detonations are produced in the inner regions of the accretion disc, thereby producing intermediate and Iron group elements. Nevertheless, the radioactive ^{56}Ni production is limited to the range of a few 10^{-4}–10^{-3} $M_{\odot}$ and could only give rise to very faint transients, with the nuclear energy providing only $\sim$1–10 per cent of the total kinetic of the ejected material. The properties of such transients suggest that to be a different class than any of the observed SNe, though they might be related to the faint tail of the observed classes of fast-evolving SNe. Their overall properties are inconsistent with those of 2005E-like type Ib faint Ca-rich SNe, and likely exclude them as progenitors of such SNe.

ACKNOWLEDGEMENTS

We acknowledge support from the Israel Science Foundation I-CORE 1829/12 grant and the Rafael Science foundation. ST acknowledges support from the Netherlands Research Council NWO (grant VENI [#639.041.645]). We thank Brian Metzger, Oded Papish, Noam Soker, Ben Margelit, and Sagiv Shiber for stimulating discussions.

REFERENCES

Chevalier R. A., 1989, ApJ, 346, 847
Cyburt R. H. et al., 2010, ApJS, 189, 240
Dan M., Rosswog S., Guillochon J., Ramirez-Ruiz E., 2012, MNRAS, 422, 2417
de Vaucouleurs G., Corwin H. G. Jr, 1985, ApJ, 295, 287
Drout M. R. et al., 2013, ApJ, 774, 58
Drout M. R. et al., 2014, ApJ, 794, 23
Fernández R., Metzger B. D., 2013, ApJ, 763, 108
Frohmaier C., Sullivan M., Maguire K., Nugent P., 2018, ApJ, 858, 50
Fryer C. L., Woosley S. E., 1998, ApJ, 502, L9
Fryer C. L., Woosley S. E., Herant M., Davies M. B., 1999, ApJ, 520, 650
Fryxell B. et al., 2000, ApJS, 131, 273
Fryxell B. A., Arnett W. D., Müller E., 1989, Bull. Am. Astron. Soc., 21, 1209
García-Senz D., Cabezón R. M., Arcones A., Relaño A., Thielemann F. K., 2013, MNRAS, 436, 3413
Houck J. C., Chevalier R. A., 1991, ApJ, 376, 234
Kasliwal M. M. et al., 2010, ApJ, 723, L98
Kasliwal M. M. et al., 2012, ApJ, 755, 161
King A., Olsson E., Davies M. B., 2007, MNRAS, 374, L34
Kushnir D., Katz B., Dong S., Livne E., Fernández R., 2013, ApJ, 778, L37
Lyman J. D., James P. A., Perets H. B., Anderson J. P., Gal-Yam A., Mazzali P., Percival S. M., 2013, MNRAS, 434, 527
Margalit B., Metzger B. D., 2016a, MNRAS, 461, 1154
Margalit B., Metzger B. D., 2016b, MNRAS, 461, 1154
Margalit B., Metzger B. D., 2017, MNRAS, 465, 2790
Meakin C. A., Seitenzahl I., Townsley D., Jordan G. C. IV, Truran J., Lamb D., 2009, ApJ, 693, 1188
Metzger B. D., 2012, MNRAS, 419, 827
Papish O., Perets H. B., 2016, ApJ, 822, 19
Paxton B. et al., 2015, ApJS, 220, 15
Paxton B., Bildsten L., Dotter A., Herwig F., Lesaffre P., Timmes F., 2011, ApJS, 192, 3
Perets H. B. et al., 2010, Nature, 465, 322
Perets H. B., Badenes C., Arcavi I., Simon J. D., Gal-yam A., 2011, ApJ, 730, 89
Poznanski D. et al., 2010, Science, 327, 58
Shakura N. I., Sunyaev R. A., 1973, A&A, 24, 337
Stone J. M., Pringle J. E., Begelman M. C., 1999, MNRAS, 310, 1002
Timmes F. X., Swesty F. D., 2000, ApJS, 126, 501
Toonen S., Perets H. B., Igoshev A. P., Michaely E., Zenati Y., 2018, A&A, 619, A53
Zenati Y., Toonen S., Perets H. B., 2018, MNRAS, 482, 1135

This paper has been typeset from a TEX/LATEX file prepared by the author.